Comprehensive analysis of central carbon metabolism reveals multiple connections between nutrients, biosynthetic capacity, and cell morphology in *Escherichia coli*

Short title: Central carbon metabolism, cell growth, and cell morphology

Corey S. Westfall[1] and Petra Anne Levin[1*]

[1] Department of Biology, Washington University, St. Louis, Missouri, U.S.A.

* Corresponding author

E-mail: plevin@wustl.edu (PAL)

Abstract

Bacterial morphology is a complex trait that is highly sensitive to changes in the environment. For heterotrophic organisms, such as *Escherichia coli*, increases in nutrient levels are frequently accompanied by several-fold increases in both size and growth rate. Despite the dramatic nature of these changes, how alterations in nutrient availability translate into changes in growth and morphology remains a largely open question. To understand the signaling networks coupling nutrient availability with size and shape, we examined the impact of deletions in the entirety of non-essential central carbon metabolic genes on *E. coli* growth rate and cell size. Our data reveal the presence of multiple metabolic nodes that play important yet distinctive roles in shaping the cell. Consistent with recent work from our lab and others, although both are sensitive to nutrient availability, size and growth rate vary independently. Cell width and length also appear to be independent phenomena, influenced by different aspects of central carbon metabolism. These findings highlight the diversity of factors that can impact cell morphology and provide a foundation for further studies.

Author summary

Often taken for granted, the shape of bacterial cells is a complex trait that is highly sensitive to environmental perturbations. Nutrients in particular, strongly impact bacterial morphology together with growth rate. The ubiquitous, rod-shaped bacteria *Escherichia coli* increases both length and width several fold upon a shift

48 from nutrient poor to nutrient rich medium, a change accompanied by an equally
49 dramatic increase in growth rate. Central carbon metabolism is an obvious site for
50 the integration of nutrient dependent signals that dictate cell size and shape. To
51 develop a clearer picture of the molecular mechanisms coupling nutrient
52 assimilation with cell growth and morphology, we screened the entirety of non-
53 essential carbon metabolic genes for their contribution to growth rate and cell
54 shape. Our data reveal the presence of multiple regulatory circuits coordinating
55 different metabolic pathways with specific aspects of cell growth and morphology.
56 Together, these data firmly establish a role for central carbon metabolism as an
57 environmentally sensitive sculptor of bacterial cells.
58

59 **Introduction**

60 The behavior and physiology of single celled organisms is at the mercy of
61 their environment. Nutrients, in particular, dramatically impact the growth rate, cell
62 cycle, and morphology of bacteria. *Salmonella typhimurium, Escherichia coli,* and
63 *Bacillus subtilis* cells cultured in nutrient rich conditions exhibit mass doubling
64 times up to 6-fold faster than their counterparts cultured in nutrient poor medium
65 [1-3]. These increases in growth rate are accompanied by similarly dramatic
66 increases in cell size. *E. coli* increases length (2-fold) and width (1.5-fold) for a ~3-
67 fold increase in total square area between nutrient poor and nutrient rich
68 conditions [3]. *B. subtilis* increases length ~3-fold in nutrient rich conditions while
69 width remains more or less constant [2,4].

The positive relationship between nutrient availability, growth rate and cell size is generally referred to as the "Growth Law". Besides cell size, DNA, RNA, and protein content of the cell also show a positive relationship with growth rate, with faster growing cells containing more of these macromolecules [1]. Although there is more total DNA/RNA/protein in larger, faster growing cells, their concentration remains relatively constant due to the concomitant increase in cell size [1,5].

Despite its name, the relationship between growth rate and cell size is complicated and there are several, well known exceptions to the Growth Law. Reducing growth rate by lowering culture temperature does not impact cell length or width, suggesting that it is nutrients rather than growth rate that determine cell size [6]. Conversely, mutations that lead to modest delays in division frequently result in increases in cell length without detectably impacting mass doubling time [7-9].

Central carbon metabolism: a hub connecting nutrient availability with growth rate and cell size

As the entry and processing point for the raw materials required for cell growth and proliferation, central carbon metabolism (CCM) plays a key role in coordinating nutrient availability with cell growth and size. Recent work indicates that CCM impacts bacterial morphology in several ways: by its impact on cell cycle progression [10-12]; by its impact on lipid synthesis [6]; and through its impact on cell wall biogenesis [13].

92 CCM-mediated changes in cell cycle progression primarily affect cell length,
93 while changes in lipid synthesis and cell wall biogenesis impact both length and
94 width. In an example of the former, UDP-glucose, produced in two steps from
95 glucose-6-phosphate at the beginning of glycolysis, stimulates interactions between
96 the moonlighting glucosyltransferase OpgH in *E. coli* and the unrelated enzyme UgtP
97 in *B. subtilis* and the essential tubulin-like cell division protein FtsZ, delaying
98 division and increasing cell length during growth in carbon rich medium [4,12]. In
99 contrast, defects in fatty acid synthesis (FAS) lead to reductions in both length and
100 width, effectively recapitulating the impact of nutrient limitation on cell morphology
101 [6,14].
102 CCM can also effect morphology via its impact on the availability of cellular
103 building blocks, particularly those required for synthesis of the cell wall. In a recent
104 study, the Young laboratory determined that defects in *wecE*, a gene encoding an
105 aminotransferase important for making the *E. coli* outer membrane molecule
106 enterobacterial common antigen (ECA), led to the formation of swollen, filamentous
107 cells. ECA is transported to the cell wall via undecaprenyl-phosphate, the lipid
108 carrier responsible for shuttling precursors for peptidoglycan and other
109 components of the bacterial cell envelope across the plasma membrane. Careful
110 genetics revealed the morphological defects associated with defects in *wecE* were
111 due to sequestration of undecaprenyl-phosphate conjugated to an ECA intermediate,
112 interfering with peptidoglycan synthesis [15].
113 More generically, nutrient starvation leads to an accumulation of the small
114 molecule guanosine tetraphosphate (ppGpp) that interacts directly with RNA

115 polymerase, to inhibit transcription of a wide array of genes, effectively curtailing
116 flux through multiple biosynthetic pathways [16]. ppGpp concentration is inversely
117 proportional to both size and growth rate: ectopic expression of the ppGpp
118 synthetase RelA during growth in nutrient rich medium reduces both growth rate
119 and cell size [6,17]. The reduction in size is indirect and dependent on ppGpp-
120 mediated inhibition of fatty acid synthesis, while the reduction in growth rate is
121 almost certainly a consequence of ppGpp-dependent inhibition of a host of essential
122 processes [6].

123 While these examples highlight several ways in which CCM might impact the
124 positive relationship between cell growth and cell morphology, they represent only
125 a small fraction of the pathways that constitute CCM. To identify additional
126 connections between nutrient levels, metabolism, and cell size in *E. coli*, we
127 screened non-essential (CCM) gene deletions for defects in cell size and growth rate.
128 Our data highlight three CCM nodes—the first branch-point of glycolysis, the
129 pentose-phosphate pathway, and acetyl-CoA metabolism—as critical links between
130 nutrient availability, cell growth and cell size. While some aspects of CCM
131 bottlenecks appear to directly impact the relationship between nutrient availability
132 and biosynthetic flux, other aspects of CCM effect growth and morphology in more
133 nuanced ways.

134

135 Results

136 Multiple connections exist between CCM, growth rate, and cell size

137 To identify key steps of CCM that impact the growth and morphology of *E.*
138 *coli*, we phenotypically analyzed cells defective in 44 non-essential CCM genes (S1
139 Table) to. These experiments took advantage of the Keio Collection, an ordered
140 insertion-deletion library of all non-essential genes in *E. coli* [18] and Coli-Inspector,
141 an Image J plug in designed for high throughput analysis of bacterial morphology
142 [19]. Prior to analysis, the Keio insertion-deletions were transduced into the
143 laboratory wild type strain MG1655. Briefly, single colonies of each mutant were
144 picked and cultured under nutrient rich conditions (Luria-Bertani (LB) broth
145 supplemented with 0.2% glucose) to an OD_{600} of ~0.2. Cultures were then back-
146 diluted to OD_{600} of 0.01 and tracked for 4 generations until they reached a maximum
147 OD_{600} of 0.2 (the low OD_{600} ensures cells are all actively growing and at
148 approximately the same growth phase prior to analysis). Cells were sampled, fixed,
149 and imaged by phase contrast microscopy. Cell size (length and width) was
150 determined using Coli-Inspector in ImageJ.
151 Based on size and mass doubling time, we assigned the 44 mutants into six
152 classes (Table 1). Represented by two mutations, Class I cells were >10% smaller
153 than wild type cells with mild to undetectable changes in growth rate (within two
154 SD of wild type mass doubling time). Eight mutations fell into Class II: small (more
155 than 10% decrease in square area than wild type) with a significant decrease in
156 doubling time (>20% wild type). Class III was heterogenous, consisting of a
157 population dominated by smaller than normal cells and punctuated by the presence
158 of a few (5-10%) very long cells. Three mutants fell into Class IV long (>10% longer
159 than WT) and two into Class V, heterogenous with a wide distribution of cell lengths

and variable cell widths (Fig 1A). Surprisingly, the majority of mutants (26) were essentially wild type with regard to growth rate and cell size (Class VI). This finding suggests the presence of alternative pathways that permit *E. coli* to bypass particular CCM enzymes and/or that nutrients that allow for bypass are present in LB. We elected not to investigate the impact of deletions in either *ppsA*, the first step of gluconeogenesis, or *fumC*, one of the three isoforms involved in the conversion of fumarate to malate in the TCA cycle, on cell size as we were unable to obtain stable MG1655 transductants of either mutant. Representative images of each mutant are shown (Fig 2).

Table 1: CCM deletion mutants exhibiting significant alterations in growth rate and/or morphology.

Gene Name	Doubling time (per minute)	Area (microns squared)	Pathway
Wild Type	22	5.1	
Class I (Small with doubling times <20% from WT)			
sucC	25	4.6	TCA Cycle
gnd	21	4.6	Pentose-Phosphate
Class II (Small and doubling times >20% from WT)			
crr	27	4.4	Glycolysis
aceE	34	2.9	Glycolysis/Acetate/Fatty acid/TCA
tktA	33	3.7	Pentose-Phosphate
pgl	26	4.5	Pentose-Phosphate
rpiA	28	3.8	Pentose-Phosphate
rpe	37	3.1	Pentose-Phosphate
pta	33	3	Acetate Metabolism
ackA	36	2.7	Acetate Metabolism
Class III (Short and Long)			
acnB	25	5.6	TCA Cycle
zwf	30	4.4	Pentose Phosphate
Class IV (Long)			
yggF	19	6.7	Putative Gluconeogensis
talB	23	5.8	Pentose-Phosphate
eda	22	6	Entner-Douderoff
Class V (heterogenous)			
tpiA	30	ND	Glycolysis
gpmM	21	ND	Glycolysis

171

172

173 Of the different classes, only the eight Class II mutants "obeyed" the Growth
174 Law, with reductions in growth rate accompanied by predictable reductions in cell
175 size (Fig 1B). The close correlation between growth rate and size for Class II
176 mutants suggests that the loss of individual genes and/or their product's catalytic
177 function, leads to a biosynthetic bottleneck that recapitulates the impact of nutrient
178 starvation on cellular physiology. In contrast, despite their heterogeneity with
179 regard to cell length, both Class I and Class IV mutants exhibited more or less
180 normal growth rates, suggesting a potential defect in the signal transduction
181 pathways coordinating CCM with cell growth and cell size. The heterogeneity of
182 Class III and Class V indicate a loss of proper regulation of cell cycle progression
183 and/or width control, leading to stochastic variations in cell morphology.

184

185 **Growth in carbon poor medium largely ameliorates CCM mutant**
186 **morphological defects**

187 To clarify the impact of nutrient flux on individual CCM mutant phenotypes,
188 we assessed the growth rate and size of Class I-V mutants in three different media:
189 LB + 0.2% glucose, the minimal media AB + 0.2% glucose, and AB + 0.2% succinate
190 representing high nutrient conditions, low nutrient glycolytic conditions, and low
191 nutrient gluconeogenic conditions respectively. Cells were measured using the
192 Matlab software package SuperSegger, which facilitates the rapid analysis of large
193 numbers of clumped cells [20]. In general, SuperSegger results corresponded almost

194 exactly with the Coli-Inspector data reported above, although cell areas were
195 smaller over all most likely due to a difference in how the two programs define cell
196 boundaries and at what point of the cell cycle that they "divide" the parent cell into
197 two daughter cells (see wild type area in Table 1 and S3 Table).

198 In light of data indicating that cells defective in *crr*, encoding the
199 phosphotransferase system subunit $EIIA^{glc}$, exhibited significant reductions in size
200 (Table 1), we also examined the nutrient dependent phenotype of cells defective for
201 adenylate cyclase or the cAMP receptor (Crp) production. Crr is part of a
202 phosphodependent transferase system that is essential for the import of glucose and
203 other sugars into *E. coli* [21]. Crr facilitates glucose import via transfer of a
204 phosphate group from Hpr to $EIIB^{glc}$ and finally to glucose, generating glucose-6-
205 phosphate at the beginning of glycolysis (reviewed in [22]). During growth on a
206 non-glycolytic substrate, phosphorylated $EIIA^{glc}$ accumulates and activates the
207 adenylate cyclase, CyaA, leading to synthesis of cyclic-AMP (cAMP) [23,24]. A co-
208 activator, cAMP binds to Crp facilitating DNA binding and stimulating transcription
209 of a broad swathe of genes including those involved in the transport and utilization
210 of non-glycolytic carbon sources [25,26]. If *crr* impacts cell size via its impact on
211 cAMP production and Crp activation, defects in both *cyaA* and *crp* should be
212 phenotypically identical to *crr* mutants with regard to cell size and growth rate. We
213 found that this is indeed true as deletions in *crr*, *cyaA*, or *crp* led to similar growth
214 rates (29, 29, and 28 minutes) and cell size (2.1 square micron area for all three
215 mutants). This implies that the growth rate and size phenotypes of *crr*::*kan* are
216 caused not by a lack of glucose import but instead by blocking cAMP synthesis.

217 Generally speaking, most of the CCM mutants retained a positive relationship
218 between nutrient availability and cell size with the exception of the three cAMP
219 mutants, *crr*::*kan*, *cyaA*::*kan*, and *crp*::*kan* (Fig 3). During growth in carbon poor
220 and/or gluconeogenic conditions, the lengths of Class I and Class II mutants
221 approached that of wild type, particularly in AB-succinate medium, and the
222 heterogeneous phenotype exhibited by mutants in Class III and Class IV was largely
223 relieved. Width also decreased, although more modestly. The average width of the
224 mutants ranged from 0.68-0.86 microns during growth in LB-glu and 0.48-0.60
225 microns during growth in AB-suc. Consistent with catabolite repression serving to
226 inhibit division during growth on a gluconeogenic carbon source, the *crp*::*kan*
227 mutants (dotted line in Fig 3B, 3C, and 3D) did not show any change in size when
228 switched from LB-glu to AB-glu. Both *crr*::*kan* and *cyaA*::*kan* (magenta and gray in
229 Fig 3) were similar to *crp*::*kan*, showing only minor, insignificant changes in length,
230 with no change in width. Unfortunately, *crr*, *cyaA*, and *crp* are essential under
231 gluconeogenic conditions, preventing analysis of these mutants in AB-succinate.
232 Although we were able to obtain cell size data for *rpiA*, *crr*, *rpe*, *aceE*, and
233 *sucA* in carbon rich (LB-glu) and carbon poor (AB-glu) conditions, all five mutants
234 were unable to grow in the gluconeogenic condition, AB + 0.2% succinate. At first
235 glance this finding appears to be in conflict with data indicating that *rpiA*, *rpe*, *aceE*,
236 and *sucA* are capable of growth in another carbon poor gluconeogenic condition: M9
237 + 0.1% glycerol [27]. However, this discrepancy likely reflects the ability of glycerol
238 to enter the CCM partway through glycolysis—as dihydroxyacetone phosphate—

239 while succinate enters through the TCA cycle, leading to dependence on different
240 pathways through CCM to synthesize all needed carbon metabolites.
241
242 **Defects in CCM differentially impact assembly of the cell division machinery**
243 To gain insight into the relationship between growth rate, cell cycle
244 progression and CCM during growth in LB-glucose, we assessed the ability of
245 different mutants to suppress the heat sensitivity associated with the GTP binding
246 defective FtsZ mutant, *ftsZ84* (G105S) [28]. While *ftsZ84* supports both FtsZ
247 assembly and division under permissive conditions (LB at 30°C), under non-
248 permissive conditions (LB with no salt at 42°C), FtsZ assembly and division are
249 blocked, leading to filamentation and cell death [7,29]. Based on extensive work
250 from our group and others, conditions or mutations that enhance FtsZ assembly are
251 expected to suppress the heat sensitivity of temperature sensitive *ftsZ* alleles
252 [4,17,30,31]. Changes in the availability of CCM products or components that
253 normally inhibit FtsZ assembly should restore growth and colony formation to
254 *ftsZ84* mutants under non-permissive conditions while defects in CCM-related
255 factors that normally promote FtsZ assembly will enhance *ftsZ84* heat sensitivity.
256 Double mutants in CCM deletions and *ftsZ84* were generated to examine the impact
257 of these mutants on FtsZ assembly.
258 Consistent with a positive impact on FtsZ assembly, the majority of Class I-V
259 mutants promoted growth of *ftsZ84* cells under mildly restrictive conditions (37°C,
260 LB no salt) (Fig 4A). The strongest suppressors were loss-of-function mutations in
261 *aceE* or *ackA* both of which increased *ftsZ84* cell viability 10,000-fold during growth

262 at 37°C on salt-free LB medium. Mild suppression was observed in loss of function
263 mutations in *crr*, *tktA*, and *pta* which increased *ftsZ84* cell viability 1,000-fold, 100-
264 fold, and 100-fold respectively. The *zwf* deletion was alone in leading to
265 enhancement of *ftsZ84*, i.e. lack of growth at 30° on LB-no salt (Fig 4B). Combined
266 with the short and long phenotype of *zwf*::*kan*, it appears that loss of *zwf* leads to
267 impairment of FtsZ activity. Significantly, we did not observe a consistent
268 correlation between reduced growth rate and suppression of *ftsZ84* heat-sensitivity
269 among the various CCM mutants.

270 As part of these experiments we also revisited the impact of a loss of function
271 mutation in *pgm*, encoding phosphoglucomutase—the enzyme that converts
272 glucose-6-phosphate to glucose-1-phosphate. In previous work, we had reported
273 that deletions in *pgm* suppress *ftsZ84* heat sensitivity [12]. However, we were
274 unable to detect any suppression of *ftsZ84* by *pgm* in this instance. Resequencing
275 BH173, the strain employed in the original study revealed acquisition of a reversion
276 mutation that restored *ftsZ84* sequence to wild type.

277 To gain a better understanding of the mechanisms coordinating central
278 carbon metabolism with cell morphology, we undertook an in depth analysis of two
279 distinctive phenotypes: the reduction in length and width observed in cells defective
280 in catabolite repression and the link between acetate metabolism, cell growth and
281 cell cycle progression revealed by defects in *aceE, ptaA, and ackA* (Fig 7). The
282 results of these efforts are described below.

283 **Catabolite-dependent regulation of FtsZ assembly and function**

284 Reasoning that if the product of *crr,* $EIIA^{glc}$, was impacting division indirectly
285 via its role in stimulation of adenylate cyclase and subsequent activation of the Crp
286 transcription factor, we hypothesized that 1) defects in either the adenylate cyclase
287 (encoded by *cya*) or *crp* should restore growth to *ftsZ84* cells under non-permissive
288 conditions, and 2) the addition of extracellular cAMP (which is able to diffuse
289 through the membrane [32]) to *crr*::*kan ftsZ84* cells should bypass *crr*::*kan* mediated
290 suppression of *ftsZ84* heat sensitivity but only in the presence of Crp. Consistent
291 with this model, deletion of either *cya* or *crp* phenocopied *crr*::*kan* mediated *ftsZ84*
292 suppression at 37°C on salt free medium (Fig 5). More directly, 5 mM cAMP was
293 sufficient to restore heat sensitivity to *crr*::*kan ftsZ84* cells as well as cells defective
294 in adenylate cyclase (*cyaA*) but only in the presence of *crp* (Fig 5). Together, these
295 data strongly argue for the presence of at least one inhibitor of FtsZ assembly within
296 the extensive Crp regulon.

297

298 **cAMP controls cell width through regulation of the morphogene *bolA***

299 In contrast to wild type cells, which decrease in both length and width upon a
300 shift from glycolytic (low cAMP) to gluconeogenic (high cAMP) conditions, the *crp*
301 deletion showed no significant changes in width when changing media from LB-glu
302 to AB-glu, suggesting a potential role for cAMP in cell width regulation (Fig 3). To
303 explore this idea, we examined the impact of extracellular cAMP on wild type
304 (MG1655) cells cultured in both glycolytic and gluconeogenic conditions.

305 Consistent with a negative impact on cell width, 5 mM exogenous cAMP was
306 sufficient to decrease wild type cell width in both LB and AB + 0.2% glucose (0.96 to
307 0.81 microns and 0.73 to 0.68 microns respectively) (Fig 6A). The addition of cAMP
308 also significantly decreased cell length (3.8 to 3.2 microns for LB and 2.7 to 2.5
309 microns for AB-Glu) and growth rate (2.7 to 2.3 doubling per hour for LB and 0.98 to
310 0.88 doublings per hour for AB-Glu) (Fig 6B). Significantly, cAMP-dependent
311 reductions in size are independent of growth rate. Reducing levels of exogenous
312 cAMP from 5 mM to 1 mM decreased the growth rate of *cyaA*::*kan* (which is unable
313 to synthesize any cAMP) in gluconeogenic conditions (AB + 0.2% succinate) from
314 0.87 to 0.79 doublings per hour, while cell width increased from 0.65 to 0.75
315 microns (Fig 6C). Although width was independent of growth rate, length was not as
316 the *cyaA*::*kan* mutant length decreased with lower cAMP from 2.6 microns in 5 mM
317 cAMP to 2.2 microns in 1 mM cAMP in a manner similar to the growth rate (Fig 6D).
318 cAMP has been implicated in the Crp dependent activation of the
319 transcription factor OmpR , which inhibits expression of a host of genes, including
320 several whose products have morphogenic activity [33]. Of particular interest is
321 *bolA*, encoding a transcription factor that inhibits transcription of *mreB* [34], which
322 encodes a key component of the elongation machinery [35]. Reductions in MreB
323 activity lead to a block in synthesis of lateral cell wall material and the formation of
324 wide and rounded cells [36,37]. *bolA* transcription has previously been shown to be
325 inhibited by addition of extracellular cAMP [38].
326 Together, genetic interactions between *crp, ompR,* and *bolA,* support a model
327 in which cAMP increases cell width indirectly, via down regulation of OmpR and the

328 concomitant increase in BolA expression leading to repression of MreB mediated
329 cell wall synthesis. Consistent with this model, cells defective in *ompR* and *bolA*
330 were refractile to the addition of exogenous cAMP with regard to cell width (Figs 6E
331 and 6F).
332
333 **Defects in acetate metabolism support links between fatty acid synthesis and**
334 **assembly of the cell division machinery**
335 Cell cycle progression is tightly correlated with growth rate in wild-type
336 cells. Fast growing cells are not only larger but contain a higher frequency of FtsZ
337 rings (Z-rings) with approximately 90% of *E. coli* cells containing visible Z-rings in
338 LB-glucose. Meanwhile, slow growing cells contain fewer Z-rings (~50%). Z-ring
339 frequency shows a roughly linear relationship to growth rate when grown in
340 different media (Fig 4C dotted line) [12,39]. Taking advantage of a green fluorescent
341 protein (GFP)-FtsZ fusion that allows us to label the FtsZ ring without detectably
342 altering size or growth [6], we assessed the frequency of FtsZ ring formation in the
343 17 mutants in Classes I through V.
344 Although the Z-ring frequency and growth rate were correlated in the
345 majority of CCM mutants, several exhibited a disconnect between these two
346 parameters, specifically those associated with acetate metabolism (black squares in
347 Fig 4C). Cells defective in *aceE*, the E1 protein of pyruvate dehydrogenase that
348 converts pyruvate to acetyl-CoA, exhibited an extremely high (86%) Z-ring
349 frequency relative to wild type cells cultured in medium of the same growth rate
350 (~75%) [12], while both *ackA* and *pta*, involved in converting acetyl-CoA to acetate,

351 exhibited lower Z-ring frequencies relative to growth rate (69% and 67%
352 respectively). Assembly of the cell division machinery is a multistep process
353 involving first, recruitment of FtsZ and other so-called early proteins to the nascent
354 division site followed by a brief delay and assembly of the late proteins, which
355 include enzymes required for synthesis of the septal cell wall (reviewed in [40]). In
356 *E. coli*, division is coincident with recruitment of FtsN, the last protein to be
357 incorporated into the division machinery and the putative "trigger" for cross wall
358 synthesis [41,42]. The two-step nature of division machinery assembly suggests two
359 potential explanations for the elevated Z-ring frequency in *aceE*::*kan* mutants: 1)
360 premature recruitment of FtsZ to the septum or 2) delays in late protein
361 recruitment and activation of cytokinesis. Conversely, the lower frequency of FtsZ
362 rings in *ackA*::*kan* and *pta*::*kan* mutants could be a consequence of either 1) delays
363 in FtsZ recruitment or 2) premature late protein recruitment and/or activation of
364 division mediated cell wall synthesis.

365 To clarify the underlying cause of the elevated Z-ring frequency in *aceE*::*kan*
366 cells and depressed Z ring frequency in the *ackA*::*kan* and *pta*::*kan* backgrounds we
367 took advantage of a heterologous, IPTG-inducible FtsN-GFP [43] to assess the
368 efficiency of FtsN recruitment in all three mutants. Growth in LB-glu showed 32% of
369 wild-type cells with FtsN-GFP localization at mid-cell (Fig 7A). In contrast, despite
370 varying Z-ring frequencies, all three mutants exhibit more or less the same
371 frequency of FtsN ring formation (24%, 23%, and 26% for *aceE*::*kan*, *ackA*::*kan*, and
372 *pta*::*kan* respectively) with all three being significantly less than wild type. The
373 consistency of FtsN ring frequency, despite differences in Z-ring frequency between

374 the three CCM mutants, suggests that it is delayed recruitment of the late division
375 proteins and/or activation of cytokinesis that is responsible for the high Z-ring
376 frequency in *aceE*::*kan* cells while the lower Z-ring frequeny in *ackA*::*kan* and
377 *pta*::*kan* mutants would appear to be a consequence of a delay in FtsZ assembly.
378 Acetyl-CoA metabolism plays a critical role in the ability of cells to synthesize
379 the wide variety of fatty acids and lipids that constitute the cell envelope [44]. *aceE*,
380 in particular, encodes a subunit of the pyruvate dehydrogenase complex responsible
381 for aerobic synthesis of the majority of acetyl-CoA, a necessary precursor in the first
382 step of FAS [45]. Defects in *aceE* are thus expected to reduce flux through FAS, and
383 based on previous work, shift the balance in lipid composition [46]. Although not
384 directly involved in FAS, defects in *pta* and *ackA* may lead to a build-up of acetyl-CoA
385 and potentially also shift flux through FAS.
386 Based on previous studies linking lipid composition to cell morphology [47],
387 we speculated defects in acetate metabolism might result in changes in plasma
388 membrane composition that interfere with assembly and activity of the cell division
389 machinery. To test this idea, we measured the Z-ring frequency of wild type and
390 mutant cells cultured in the presence of sub-inhibitory concentrations of the fatty
391 acid synthesis inhibitor triclosan (50 ng/mL). This concentration is too low to
392 impact growth rate but has a modest positive impact on cell size [6]. Triclosan
393 inhibits FabI, the enzyme that catalyzes the reduction of enoyl-ACP during the
394 elongation cycle of fatty acid synthesis [48]. Although not a perfect recapitulation of
395 a block upstream of acetyl-CoA synthesis, as it blocks a downstream step, both

396 triclosan treatment and the *aceE* mutations should similarly curtail flux through
397 FAS.
398 In support of a model in which modest reductions in flux through FAS
399 negatively impact assembly of the cell division machinery, Z-ring frequency was
400 significantly increased in wild type cells as well as in *aceE*::*kan, pta*::*kan*, and
401 *ackA*::*kan* cells during growth in sub-MIC (minimum inhibitory concentration), 50
402 ng/mL triclosan. (Z-ring frequency: wild type 88% +T/95% -T; *pta*::*kan* 56% -T/
403 79% + T; *ackA*::*kan* 60% -T/74% +T; *aceE*::*kan* 79% -T to 87% +T) (Fig 7B). *pta* or
404 *ackA* deletion mutants were slightly more sensitive to triclosan with regard to Z-ring
405 frequency than either *aceE* or wild type cells, likely a reflection of the already high
406 frequency of FtsZ rings in these latter strains.
407 Further supporting a positive connection between FAS and assembly of the
408 cell division machinery, 50 ng/mL triclosan enhanced the heat sensitive phenotype
409 of conditional mutations in several cell division genes including *ftsA* (*ftsA27*-an
410 early, actin-like protein), *ftsK* (*ftsK44*—a late division protein involved in
411 chromosome partitioning), *ftsQ* (*ftsQ1*—a late division protein believed to serve
412 primarily as a scaffold), and *ftsI* (*ftsI23*—a late division protein with a trans-
413 peptidase domain) [49-52]. Somewhat surprisingly given its impact on FtsZ ring
414 frequency (Fig 7B), triclosan had no impact on the heat-sensitivity of *ftsZ84* (Fig 7C).
415 We speculate that the differential impact of triclosan on *ftsZ84* relative to the other
416 conditional mutants is a consequence of their subcellular location (cytoplasmic –
417 FtsZ) versus membrane associated (FtsA) and integrated into the membrane (FtsQ,
418 FtsK, and FtsI) [40].

419 ## Discussion

420 Our systematic analysis of the relationship between central carbon
421 metabolism, cell growth, and cell size both reinforces the Growth Law as a general
422 principal (i.e. growth rate and size are positively correlated) but also calls into
423 question many of the fundamental assumptions that underlie it. While the largest
424 class of mutants with observable phenotypes—Class II: small with reduced growth
425 rates, essentially "obeyed" the law so to speak, growth rate and size varied
426 independently in the other classes of CCM mutants (Fig 1B). Class II mutants closely
427 resemble cells cultured in nutrient-poor conditions with regard to growth rate and
428 size, suggesting these cells are experiencing a near global reduction in biosynthetic
429 capacity. In contrast, growth rate and morphology are independent of one another
430 in the other nine CCM mutants (Table 1), consistent with defects in specific
431 regulatory or structural functions that directly impact cell length and/or width.

432 These results are in line with accumulating work indicating that growth rate
433 and cell size are independent phenomena. Modest defects in cell division are well
434 known to increase bacterial cell size—particularly length—without impacting
435 growth rate [4,7,50,51,53], while defects in transcription severely curtail growth but
436 have little detectable impact on morphology [6]. Most importantly, an exhaustive
437 phenotypic analysis of the entirety of non-essential genes in *E. coli* by the Jacobs-
438 Wagner group, failed to identify any evidence supporting a direct connection
439 between growth rate and size [54].

440

441

442 **Overflow metabolism and cell size**

443 In a common, yet paradoxical, fermentative mechanism known as "overflow
444 metabolism", *E. coli* convert up to 50% of available glucose into acetate during
445 aerobic growth in nutrient rich conditions [55] . Acetate fermentation is inefficient,
446 resulting in ~14 fewer ATP per glucose than oxidative phosphorylation and, unlike
447 other fermentative pathways, does not regenerate NAD^+ from NADH [56]. While it is
448 unclear why bacteria perform overflow metabolism, it is potentially a more
449 proteome-efficient means of moving carbon through CCM, ensuring that glycolysis
450 proceeds at a maximum pace when nutrients are plentiful.

451 Supporting the idea that overflow metabolism is critical for maximizing
452 glycolytic flux, defects in *pta*, *ackA,* and *aceE*, encoding the first two enzymes in
453 acetate fermentation and a subunit of pyruvate dehydrogenase respectively, are
454 dramatically impaired in both growth rate and cell size. This is consistent with a
455 global reduction in biosynthetic capacity. Whether this reduction is the result of
456 lower ATP production or the consequence of a bottleneck in flux through critical
457 biosynthetic pathways is unclear. Regardless, we suspect that reductions in ATP
458 levels and/or biosynthesis indirectly result in accumulation of the alarmone ppGpp
459 [57], providing an explanation for the observed suppression of *ftsZ84* heat-
460 sensitivity in *pta, ackA,* and *aceE* deletion strains. Increases in ppGpp are well
461 known to suppress the conditional nature of *ftsZ84,* although the precise mechanism
462 has yet to be determined [17,58] .

463

464

465 **cAMP is a key player in maintaining the correct cellular aspect ratio**

466 A somewhat surprising finding is the identification of cAMP as a contributor
467 to nutrient dependent reduction in both cell length and width. Accumulating under
468 gluconeogenic conditions, cAMP binds to the transcriptional activator Crp and
469 regulates expression of more the than 280 genes [59]. Although the precise
470 member(s) of the cAMP-Crp regulon responsible remains elusive, our data indicate
471 that cAMP-Crp function together to reduce width under nutrient poor conditions via
472 their impact on the morphogenic factor BolA and cell length via its impact on the
473 assembly of FtsZ (Figs 5 and 6). In this regard, cAMP differs from metabolic
474 signaling molecule, ppGpp, which genetics indicate is a positive regulator of division
475 (Fig 8).

476

477 **CCM is robust but not necessarily efficient**

478 Perhaps the biggest surprise of this study is our finding that the defects in the
479 majority of non-essential CCM genes had little to no detectable impact on either cell
480 size or growth rate. While the lack of phenotype in many cases is likely a
481 consequence of our screening conditions, nutrient-rich, complex medium
482 supplemented with glucose, in certain cases the robust growth we observed is
483 difficult to explain. For example, we anticipated that defects in phosphoglucose
484 isomerase (encoded by *pgi*), the first dedicated step in glycolysis would dramatically
485 impact growth rate and size by virtue of its impact on not only glycolysis, but also
486 other associated pathways leading to reductions in ATP synthesis and overall
487 biosynthetic capacity [60]. Instead, we were unable to distinguish *pgi* mutants from

488 wild type cells during growth LB-glucose (Table S2). Based on our identification of
489 seven mutants in the pentose-phosphate pathway, we hypothesize that despite the
490 ubiquitous nature of glycolysis in nutrient- rich medium, glucose is predominantly
491 driven through the pentose-phosphate pathway to generate essential building
492 blocks.

493 Similarly, we observed little in the way of a detectable phenotype associated
494 with defects in the gene encoding citrate synthase *gltA*. Essential for the complete
495 oxidation of carbon, GltA synthesizes citrate from oxaloacetate and acetyl-CoA at the
496 entry point into the TCA cycle [61]. Despite its seeming importance, previous work
497 indicates that *E. coli* represses *gltA* transcription in the presence of glucose,
498 suggesting that it can forgo complete carbon oxidation under nutrient rich
499 conditions [59,62]. It may be that under nutrient rich condition, *E. coli* maximizes
500 rapid growth over the efficient use of available carbon, a proposition that is in line
501 with our data indicating that defects in acetate metabolism significantly curtail
502 growth in nutrient rich medium (Table 1).

503

504 **Concluding thoughts**

505 While this screen demonstrates the ability of systematic phenotypic analysis
506 to identify new connections between CCM, cell growth and cell size, many questions
507 remain unanswered. In addition to the large number of insertion mutants with no
508 observable phenotype, defects in 17 genes resulted in dramatic changes in growth
509 rate and cell morphology. Of these, we were able to identify the proximal cause in
510 24% (*crr*, *aceE*, *pta*, *ackA*; Figs 5-7). A better understanding of the remaining 13

511 mutations will likely require a combination of genetics and metabolomics to tease
512 apart the root cause of their morphological and growth related defects.
513 Additionally, although this effort focused specifically on carbon metabolism,
514 the availability of other nutrients—particularly nitrogen, phosphorous, sulfur and
515 iron— have also been implicated in growth and morphology. Assessing the
516 phenotype of the CCM insertion collection under conditions in which these factors
517 are limiting is thus also worthwhile. Finally, *E. coli* is believed to spend much of its
518 time under microaerobic or anaerobic conditions. Understanding how oxygen levels
519 impact growth, cell cycle progression, and cell morphology thus remains a
520 tantalizingly open question.
521

522 Materials and Methods

523 Strains and media

524 All chemicals, media components, and antibiotics were purchased from
525 Sigma-Aldrich (St. Louis, MO). *E. coli* strains were constructed through standard P1
526 vir transductions [63] moving kanamycin marked insertion deletions from Keio
527 collection strains [18] purchased from the Coli Genomic Stock Center into MG1655
528 (F^- λ^- *ilvG*- *rfb*-50 *rph*-1), our "wild type" parental strain. Cell were cultured in Luria-
529 Bertani (LB) broth supplemented with 0.2% glucose or AB defined media [64]
530 supplemented with either 0.2% glucose or 0.2% succinate as the sole carbon source.
531 Unless otherwise noted (e.g. for heat sensitive conditional alleles of cell division
532 genes including *ftsZ84*, *ftsA27*, *ftsK44*, *ftsQ1*, and *ftsI23*), cells were cultured at 37° C
533 and sampled for analysis at OD_{600} between 0.1 and 0.2. For the primary analysis cells

534 were cultured in 5 mL LB + 0.2% glucose and aerated at 200 rpm. For measuring the
535 effect of different media, cells were cultured in 200 µL of specified media in a 96-
536 well plate and aerated at 567 rpm in a BioTek© Eon© plate reader (Fig 3).
537

538 **Microscopy**

539 Cells were sampled directly from cultures and fixed in 16%
540 paraformaldehyde (Electron Microscopy Sciences) as described [6]. Fixed cells were
541 mounted on agarose pads and visualized using a 100x phase-fluor objective on a
542 Nikon© Ti-E inverted microscope. To facilitate visualization of FtsZ rings, 1 mM IPTG
543 was added to cultures of cells encoding a chromosomal P_{IPTG}-*ftsZ-GFP* [65].
544 Expression of a chromosomal P_{IPTG}-*ftsN-GFP* was induced with 50 µM IPTG [43]. GFP
545 fluorescence was detected with a C-FL GFP filter cube with 470/40nm excitation
546 and 525/50nm emission (Chroma Technology Corporation) Nikon Elements
547 software (Nikon Instruments, Inc.) was used for image capture and analysis. >200
548 cells were counted per experimental replicate and at least three independent
549 replicates were used for each data point.
550

551 **Cell Size Measurements**

552 Cell size from phase-contrast images was determined with one of two freely
553 available segmentation software packages: the ImageJ© plug-in Coli Inspector [19]
554 (Fig 1, Tables 1 and S2) or SuperSegger, a MatLab© based application [20] (Figs 3-7,
555 Table S3). As Coli Inspector does not determine area directly, we estimated it as
556 length x width. SuperSegger directly determines the area of individual cells. We

557 determined the area of ≥100 cells for each experiment and/or condition. Unless
558 otherwise noted, average size was determined from 3 independent experiments.
559
560 **Dot plating efficiency assays**
561 Heat-sensitive cell division alleles, *ftsZ84*, *ftsA27*, *ftsK44*, *ftsQ1*, and *ftsI23*
562 were cultured in LB at 30°C degrees to an OD_{600} of ~0.5. 1 mL of cells were then
563 pelleted, washed once with LB-no salt, and re-suspended to an OD_{600} of 0.1 in LB-no
564 salt. 10 µL of serial dilutions between 10^{-1} to 10^{-6} were plated under permissive
565 conditions (LB at 30°C) or non-permissive conditions (LB-no salt at 37°C). Due to
566 the strains extreme sensitivity, LB-no salt at 30°C was non-permissive for *zwf*::*kan*
567 *ftsZ84* double mutants. For cAMP or triclosan addition experiments, 5 mM cAMP or
568 50 ng/mL triclosan was added directly to LB agar prior to pouring the plates. Each
569 plating efficiency experiment was repeated three times with representative images
570 shown.
571

572 ## Acknowledgements

573 We would like to thank the Coli Genetic Stock Center (CGSC) for providing
574 numerous strains quickly. We'd like to thank Norbert Vischer for aid in using Coli
575 Inspector and Stella Stylianidou and Paul Wiggins for help with SuperSegger. We
576 would like to thank Elizabeth Mueller for work on the *pgm ftsZ84* double mutant.
577 We would also like to thank Elizabeth Mueller, Dr. Ashley Sherp, and the Hani Zaher
578 laboratory for critical feedback on this work.
579

580 **References**

581 1. Schaechter M, Maaløe O, Kjeldgaard NO. Dependency on medium and
582 temperature of cell size and chemical composition during balanced grown of
583 Salmonella typhimurium. J Gen Microbiol. 1958;19: 592–606.

584 2. Sargent MG. Control of cell length in Bacillus subtilis. J Bacteriol. 1975;123: 7–
585 19.

586 3. Donachie WD, Begg KJ. Cell length, nucleoid separation, and cell division of
587 rod-shaped and spherical cells ofEschericia coli. J Bacteriol. 1989;171: 4633–
588 4639.

589 4. Weart RB, Lee AH, Chien A-C, Haeusser DP, Hill NS, Levin PA. A metabolic
590 sensor governing cell size in bacteria. Cell. 2007;130: 335–347.
591 doi:10.1016/j.cell.2007.05.043

592 5. Donachie WD. Relationship between cell size and time of initiation of DNA
593 replication. Nature. 1968;219: 1077–9.

594 6. Vadia S, Jessica LT, Lucena R, Yang Z, Kellogg DR. Fatty Acid Availability Sets
595 Cell Envelope Capacity and Dictates Microbial Cell Size. Current Biology. 2017.

596 7. Arjes HA, Lai B, Emelue E, Steinbach A, Levin PA. Mutations in the bacterial
597 cell division protein FtsZ highlight the role of GTP binding and longitudinal
598 subunit interactions in assembly and function. BMC Microbiol. 2015;15: 209.
599 doi:10.1186/s12866-015-0544-z

600 8. Coltharp C, Buss J, Plumer TM, Xiao J. Defining the rate-limiting processes of
601 bacterial cytokinesis. Proc Natl Acad Sci USA. 2016;113: E1044–53.
602 doi:10.1073/pnas.1514296113

603 9. Zheng H, Ho P-Y, Jiang M, Bin Tang, Liu W, Li D, et al. Interrogating the
604 Escherichia coli cell cycle by cell dimension perturbations. P Natl Acad Sci
605 USA. 2016;113: 15000–15005.

606 10. Tymecka-Mulik J, Boss L, Maciąg-Dorszyńska M, Rodrigues JFM, Gaffke L,
607 Wosinski A, et al. Suppression of the Escherichia coli dnaA46 mutation by
608 changes in the activities of the pyruvate-acetate node links DNA replication
609 regulation to central carbon metabolism. Korolev S, editor. PLoS ONE. Public
610 Library of Science; 2017;12: e0176050. doi:10.1371/journal.pone.0176050

611 11. Monahan LG, Hajduk IV, Blaber SP, Charles IG, Harry EJ. Coordinating
612 bacterial cell division with nutrient availability: a role for glycolysis. MBio.
613 2014;5. doi:10.1128/mBio.00935-14

614 12. Hill NS, Buske PJ, Shi Y, Levin PA. A Moonlighting Enzyme Links Escherichia

615 coli Cell Size with Central Metabolism. PLoS Genet. Public Library of Science;
616 2013;9: e1003663. doi:10.1371/journal.pgen.1003663

617 13. Irnov I, Wang Z, Jannetty ND, Bustamante JA, Rhee KY, Jacobs-Wagner C.
618 Crosstalk between the tricarboxylic acid cycle and peptidoglycan synthesis in
619 Caulobacter crescentus through the homeostatic control of α-ketoglutarate.
620 Casadesús J, editor. PLoS Genet. Public Library of Science; 2017;13: e1006978.
621 doi:10.1371/journal.pgen.1006978

622 14. Yao Z, Davis RM, Kishony R, Kahne D, Ruiz N. Regulation of cell size in
623 response to nutrient availability by fatty acid biosynthesis in Escherichia coli.
624 Proc Natl Acad Sci USA. 2012;109: E2561–8. doi:10.1073/pnas.1209742109

625 15. Jorgenson MA, Kannan S, Laubacher ME, Young KD. Dead-end intermediates
626 in the enterobacterial common antigen pathway induce morphological defects
627 in Escherichia coli by competing for undecaprenyl phosphate. Mol Microbiol.
628 2015;100: 1–14. doi:10.1111/mmi.13284

629 16. Magnusson LU, Farewell A, Nyström T. ppGpp: a global regulator in
630 Escherichia coli. Trends in Microbiology. 2005.

631 17. Powell BS, Court DL. Control of ftsZ expression, cell division, and glutamine
632 metabolism in Luria-Bertani medium by the alarmone ppGpp in Escherichia
633 coli. J Bacteriol. 1998;180: 1053–1062.

634 18. Baba T, Ara T, Hasegawa M, Takai Y, Okumura Y, Baba M, et al. Construction of
635 Escherichia coli K-12 in-frame, single-gene knockout mutants: the Keio
636 collection. Mol Syst Biol. EMBO Press; 2006;2: 2006.0008.
637 doi:10.1038/msb4100050

638 19. Vischer NOE, Verheul J, Postma M, van den Berg van Saparoea B, Galli E,
639 Natale P, et al. Cell age dependent concentration of Escherichia coli divisome
640 proteins analyzed with ImageJ and ObjectJ. Front Microbiol. 2015;6: 586.
641 doi:10.3389/fmicb.2015.00586

642 20. Stylianidou S, Brennan C, Nissen SB, Kuwada NJ, Wiggins PA. SuperSegger:
643 robust image segmentation, analysis and lineage tracking of bacterial cells.
644 Mol Microbiol. 2016;102: 690–700. doi:10.1111/mmi.13486

645 21. Gabor E, Göhler A-K, Kosfeld A, Staab A, Kremling A, Jahreis K. The
646 phosphoenolpyruvate-dependent glucose-phosphotransferase system from
647 Escherichia coli K-12 as the center of a network regulating carbohydrate flux
648 in the cell. Eur J Cell Biol. 2011;90: 711–720. doi:10.1016/j.ejcb.2011.04.002

649 22. Deutscher J, Francke C, Postma PW. How phosphotransferase system-related
650 protein phosphorylation regulates carbohydrate metabolism in bacteria.
651 Microbiol Mol Biol Rev. American Society for Microbiology; 2006;70: 939–

652 1031. doi:10.1128/MMBR.00024-06

653 23. Saier MH, Feucht BU, Hofstadter LJ. Regulation of carbohydrate uptake and
654 adenylate cyclase activity mediated by the enzymes II of the
655 phosphoenolpyruvate: sugar phosphotransferase system in Escherichia coli. J
656 Biol Chem. American Society for Biochemistry and Molecular Biology;
657 1976;251: 883–892.

658 24. Park Y-H, Lee BR, Seok Y-J, Peterkofsky A. In vitro reconstitution of catabolite
659 repression in Escherichia coli. J Biol Chem. American Society for Biochemistry
660 and Molecular Biology; 2006;281: 6448–6454. doi:10.1074/jbc.M512672200

661 25. Zubay G, Schwartz D, Beckwith J. Mechanism of activation of catabolite-
662 sensitive genes: a positive control system. P Natl Acad Sci USA. National
663 Academy of Sciences; 1970;66: 104–110.

664 26. Grainger DC, Hurd D, Harrison M, Holdstock J, Busby SJW. Studies of the
665 distribution of Escherichia coli cAMP-receptor protein and RNA polymerase
666 along the E. coli chromosome. P Natl Acad Sci USA. National Acad Sciences;
667 2005;102: 17693–17698. doi:10.1073/pnas.0506687102

668 27. Joyce AR, Reed JL, White A, Edwards R, Osterman A, Baba T, et al.
669 Experimental and computational assessment of conditionally essential genes
670 in Escherichia coli. J Bacteriol. American Society for Microbiology; 2006;188:
671 8259–8271. doi:10.1128/JB.00740-06

672 28. Ricard M, Hirota Y. Process of cellular division in Escherichia coli:
673 physiological study on thermosensitive mutants defective in cell division. J
674 Bacteriol. 1973;116: 314–322.

675 29. Addinall SG, Lutkenhaus CJ. Temperature shift experiments with anftsZ84(Ts)
676 strain reveal rapid dynamics of FtsZ localization and indicate that the Z ring is
677 required throughout septation and cannot reoccupy division sites once
678 constriction has initiated. J Bacteriol. 1997;179: 4277–4284.

679 30. Levin PA, Kurtser IG, Grossman AD. Identification and characterization of a
680 negative regulator of FtsZ ring formation in Bacillus subtilis. P Natl Acad Sci
681 USA. 1999;96: 9642–9647.

682 31. Gervais FG, Drapeau GR. Identification, cloning, and characterization of rcsF, a
683 new regulator gene for exopolysaccharide synthesis that suppresses the
684 division mutation ftsZ84 in Escherichia coli K-12. J Bacteriol. 1992;174: 8016–
685 8022.

686 32. Jackson DW, Simecka JW, Romeo T. Catabolite repression of Escherichia coli
687 biofilm formation. J Bacteriol. American Society for Microbiology (ASM);
688 2002;184: 3406–3410. doi:10.1128/JB.184.12.3406-3410.2002

689 33. Huang L, Tsui P, Freundlich M. Positive and negative control of ompB
690 transcription in Escherichia coli by cyclic AMP and the cyclic AMP receptor
691 protein. J Bacteriol. American Society for Microbiology (ASM); 1992;174: 664–
692 670.

693 34. Yamamoto K, Nagura R, Tanabe H, Fujita N, Ishihama A, Utsumi R. Negative
694 regulation of the bolA1p of Escherichia coli K-12 by the transcription factor
695 OmpR for osmolarity response genes. FEMS Microbiol Lett. 2000;186: 257–
696 262.

697 35. Doi M, Wachi M, Ishino F, Tomioka S, Ito M, Sakagami Y, et al. Determinations
698 of the DNA sequence of the mreB gene and of the gene products of the mre
699 region that function in formation of the rod shape of Escherichia coli cells. J
700 Bacteriol. American Society for Microbiology; 1988;170: 4619–4624.
701 doi:10.1128/jb.170.10.4619-4624.1988

702 36. Kruse T, Bork-Jensen J, Gerdes K. The morphogenetic MreBCD proteins of
703 Escherichia coli form an essential membrane-bound complex. Mol Microbiol.
704 Blackwell Publishing Ltd; 2005;55: 78–89. doi:10.1111/j.1365-
705 2958.2004.04367.x

706 37. Divakaruni AV, Baida C, White CL, Gober JW. The cell shape proteins MreB and
707 MreC control cell morphogenesis by positioning cell wall synthetic complexes.
708 Mol Microbiol. 2007 ed. 2007;66: 174–188. doi:10.1111/j.1365-
709 2958.2007.05910.x

710 38. Lange R, Hengge-Aronis R. Growth phase-regulated expression of bolA and
711 morphology of stationary-phase Escherichia coli cells are controlled by the
712 novel sigma factor sigma S. J Bacteriol. 1991;173: 4474–4481.

713 39. Weart RB, Levin PA. Growth rate-dependent regulation of medial FtsZ ring
714 formation. J Bacteriol. 2003;185: 2826–2834.

715 40. Margolin W. FtsZ and the division of prokaryotic cells and organelles. Nat Rev
716 Mol Cell Biol. 2005;6: 862–871.

717 41. Lutkenhaus J. FtsN--trigger for septation. J Bacteriol. 2009;191: 7381–7382.
718 doi:10.1128/JB.01100-09

719 42. Daley DO, Skoglund U, Söderström B. FtsZ does not initiate membrane
720 constriction at the onset of division. Sci Rep. 2016;6: 33138.
721 doi:10.1038/srep33138

722 43. Gerding MA, Liu B, Bendezú FO, Hale CA, Bernhardt TG, de Boer PAJ. Self-
723 enhanced accumulation of FtsN at Division Sites and Roles for Other Proteins
724 with a SPOR domain (DamX, DedD, and RlpA) in Escherichia coli cell
725 constriction. J Bacteriol. 2009;191: 7383–7401. doi:10.1128/JB.00811-09

726 44. Parsons JB, Rock CO. Bacterial lipids: Metabolism and membrane homeostasis.
727 Progress in Lipid Research. 2013;52: 249–276.
728 doi:10.1016/j.plipres.2013.02.002

729 45. Li M, Ho PY, Yao S, Shimizu K. Effect of lpdA gene knockout on the metabolism
730 in Escherichia coli based on enzyme activities, intracellular metabolite
731 concentrations and metabolic flux analysis by .... Journal of biotechnology.
732 2006.

733 46. Buttke TM, Ingram L. Inhibition of unsaturated fatty acid synthesis in
734 Escherichia coli by the antibiotic cerulenin. Biochemistry. 1978.

735 47. Rowlett VW, Mallampalli VKPS, Karlstaedt A, Dowhan W, Taegtmeyer H,
736 Margolin W, et al. Impact of Membrane Phospholipid Alterations in
737 Escherichia coli on Cellular Function and Bacterial Stress Adaptation.
738 jbasmorg.

739 48. McMurry LM, Oethinger M, Levy SB. Triclosan targets lipid synthesis. Nature.
740 1998;394: 531–532. doi:10.1038/28970

741 49. Herricks JR, Nguyen D, Margolin W. A thermosensitive defect in the ATP
742 binding pocket of FtsA can be suppressed by allosteric changes in the dimer
743 interface. Mol Microbiol. 2014;94: 713–727. doi:10.1111/mmi.12790

744 50. Begg KJ, Dewar SJ, Donachie WD. A new Escherichia coli cell division gene,
745 ftsK. J Bacteriol. American Society for Microbiology; 1995;177: 6211–6222.
746 doi:10.1128/jb.177.21.6211-6222.1995

747 51. Storts DR, Aparicio OM, Schoemaker JM, Markovitz A. Overproduction and
748 identification of the ftsQ gene product, an essential cell division protein in
749 Escherichia coli K-12. J Bacteriol. American Society for Microbiology (ASM);
750 1989;171: 4290–4297.

751 52. Begg KJ, Donachie WD. Cell shape and division in Escherichia coli:
752 experiments with shape and division mutants. J Bacteriol. 1985;163: 615–
753 622.

754 53. Labie C, Bouche F, Bouche JP. Isolation and mapping of Escherichia coli
755 mutations conferring resistance to division inhibition protein DicB. J
756 Bacteriol. 1989;171: 4315–4319.

757 54. Campos M, Dobihal GS, Jacobs-Wagner C. Genome-wide phenotypic analysis of
758 growth, cell morphogenesis and cell cycle events in Escherichia coli. bioRxiv.
759 Cold Spring Harbor Labs Journals; 2017;: 101832. doi:10.1101/101832

760 55. Aristidou AA, San KY, Bennett GN. Metabolic engineering of Escherichia coli to
761 enhance recombinant protein production through acetate reduction.

762 Biotechnol Prog. American Chemical Society; 1995;11: 475–478.
763 doi:10.1021/bp00034a019

764 56. Basan M, Hui S, Okano H, Zhang Z, Shen Y. Overflow metabolism in Escherichia
765 coli results from efficient proteome allocation. Nature. Nature Publishing
766 Group; 2015;528: 99–104.

767 57. Liu K, Bittner AN, Wang JD. Diversity in (p)ppGpp metabolism and effectors.
768 Curr Opin Microbiol. 2015;24C: 72–79. doi:10.1016/j.mib.2015.01.012

769 58. Navarro F, Robin A, D'Ari R, Joseleau-Petit D. Analysis of the effect of ppGpp
770 on the ftsQAZ operon in Escherichia coli. Mol Microbiol. 1998;29: 815–823.

771 59. Zheng D, Constantinidou C, Hobman JL, Minchin SD. Identification of the CRP
772 regulon using in vitro and in vivo transcriptional profiling. Nucleic Acids Res.
773 2004;32: 5874–5893. doi:10.1093/nar/gkh908

774 60. Adhya S, Schwartz M. Phosphoglucomutase mutants of Escherichia coli K-12. J
775 Bacteriol. 1971;108: 621–626.

776 61. Spencer ME, Guest JR. Molecular cloning of four tricarboxylic acid cyclic genes
777 of Escherichia coli. J Bacteriol. American Society for Microbiology (ASM);
778 1982;151: 542–552.

779 62. Walsh K, Koshland DE. Characterization of rate-controlling steps in vivo by
780 use of an adjustable expression vector. P Natl Acad Sci USA. National Acad
781 Sciences; 1985;82: 3577–3581.

782 63. Lennox ES. Transduction of linked genetic characters of the host by
783 bacteriophage P1. Virology. 1955;1: 190–206.

784 64. Clark DJ, Maaløe O. DNA replication and the division cycle in Escherichia coli. J
785 Mol Biol. 1967.

786 65. Hale CA, de Boer PA. Recruitment of ZipA to the septal ring of Escherichia coli
787 is dependent on FtsZ and independent of FtsA. J Bacteriol. 1999;181: 167–
788 176.

789

790

791

792 ## Figure Legends

793 **Figure 1: The effect of central carbon metabolic gene deletions on cell growth**
794 **and size.** (A) Mutant phenotypes mapped onto central carbon metabolic pathways.
795 Arrows are colored based on the phenotype as follows: black= normal growth and
796 size; green = normal growth and small size (<10% smaller than WT); red = slow
797 growth (>20% increase in doubling time) and small size; orange = normal growth
798 and long cells (>10% larger than WT); blue = short and long cells; purple = highly
799 variable size; and dotted lines = essential genes. Brown arrows correspond to
800 deletions that obtained suppressor mutations rapidly and were not analyzed. (B)
801 Relationship between cell area and growth rate, as doublings per hour. Icons are
802 colored as in panel (A).
803
804 **Figure 2: Representative images of all CCM mutants exhibiting morphology**
805 **distinct from the wild type parental strain.** Merged images of morphologically
806 distinct CCM mutant strains expressing an *ftsZ-GFP* fusion to permit visualization of
807 the cytokinetic ring. Scale bar = 5 microns and is the same for all images.
808
809 **Figure 3: CCM deletions exhibit medium-dependent effects on growth and**
810 **morphology.** (A) Cell size versus growth rate in LB-glucose (black diamonds), AB-
811 glucose (orange triangles), and AB-succinate (blue circles). Length (B), width (C),
812 and area (D) are plotted for each mutant in the three different media. Dotted line =
813 *crp*::*kan* in LB-glucose and AB-glucose.
814

815 **Figure 4: CCM mutations differentially impact FtsZ localization and activity.**
816 (A) Dot-plating efficiencies of the CCM deletion *ftsZ84* double mutants cultured
817 under permissive (LB, 30°C) and non-permissive (LB-no salt, 37°C) conditions. (B)
818 Dot-plating efficiency of *zwf*::*kan ftsZ84* double mutant. Note the reduction in
819 *zwf*::*kan ftsZ84* viability under intermediate growth conditions (30°C on LB-no salt).
820 (C) FtsZ ring frequency versus growth rate for the CCM mutants. For reference we
821 have included previously reported data on the relationship between nutrient
822 availability and FtsZ ring frequency (dotted black line) [12]. Mutants are grouped
823 by metabolic pathway: black squares = acetyl-CoA production and acetate
824 fermentation; green triangles = pentose-phosphate shunt; purple diamonds = TCA
825 cycle; orange circle = Entner-Doudoroff pathway; blue cross = cAMP synthesis; and
826 red plus = gluconeogenesis.
827
828 **Figure 5: Loss of cAMP signaling suppresses *ftsZ84* heat-sensitivity.**
829 Representative dot-plating efficiencies of *ftsZ84* alone or in combination with
830 insertion deletions in cAMP signaling genes *crr*, *cyaA*, and *crp*. Cells were plated on
831 and grown at permissive (LB, 30°C), non-permissive (LB-no salt, 37°C), and non-
832 permissive containing cAMP (LB-no salt + 5mM cAMP, 37°C) conditions.
833
834 **Figure 6: cAMP signaling reduces cell width via the morphogenic transcription**
835 **factor, *bolA*.** Wild-type MG1655 cell size was measured with and without
836 exogenous 5 mM cAMP in either LB or AB-glucose. Width is shown in (A) and length
837 in (B). Width (C) and length (D) of *cyaA*::*kan* grown in AB-succinate with different

838 levels of exogenous cAMP shows that width is not correlated with growth rate but
839 length is. (E) Deletions in *crp*, *ompR*, or *bolA* abolish the cAMP-dependent cell
840 reductions in cell width. (F) Proposed genetic pathway linking cAMP to cell width.
841
842 **Figure 7: Partial inhibition of fatty acid synthesis negatively impacts assembly**
843 **and activity of the late division proteins.** (A). FtsN septal localization was
844 measured in MG1655, *aceE*::*kan*, *ackA*::*kan*, and *pta*::*kan* expressing an *ftsN-GFP*
845 from an IPTG inducible promoter (B.) FtsZ-ring frequency was measured MG1655,
846 *aceE*::*kan*, *ackA*::*kan*, and *pta*::*kan* cells expressing *ftsZ-GFP* from an IPTG-inducible
847 promoter. Cells were cultured with (gray) or without (black) 50 ng/mL triclosan. (C)
848 Representative plating efficiencies of wild-type cells and the heat-sensitive cell
849 division mutants *ftsZ84*, *ftsA27*, *ftsK44*, and *ftsQ1* cultured on LB at 37°C with or
850 without triclosan. *ftsI23* was plated on LB-no salt at 37°C with or without triclosan.
851
852 **Figure 8: Proposed pathway linking nutrient levels to cell length and width**
853 **through the signaling nucleotides cAMP and ppGpp.**
854
855 ## Supporting Information
856 **Table S1. List of bacterial strains used in this study**
857
858 **Table S2. Raw size and growth rate data for all central carbon metabolic gene**
859 **deletions.**
860

861 **Table S3. Raw data for figure 3 (CCM mutant growth in different media).**

862

863 **Table S4. Raw data for figure 4C (Z-ring frequency of CCM mutants).**

864

865

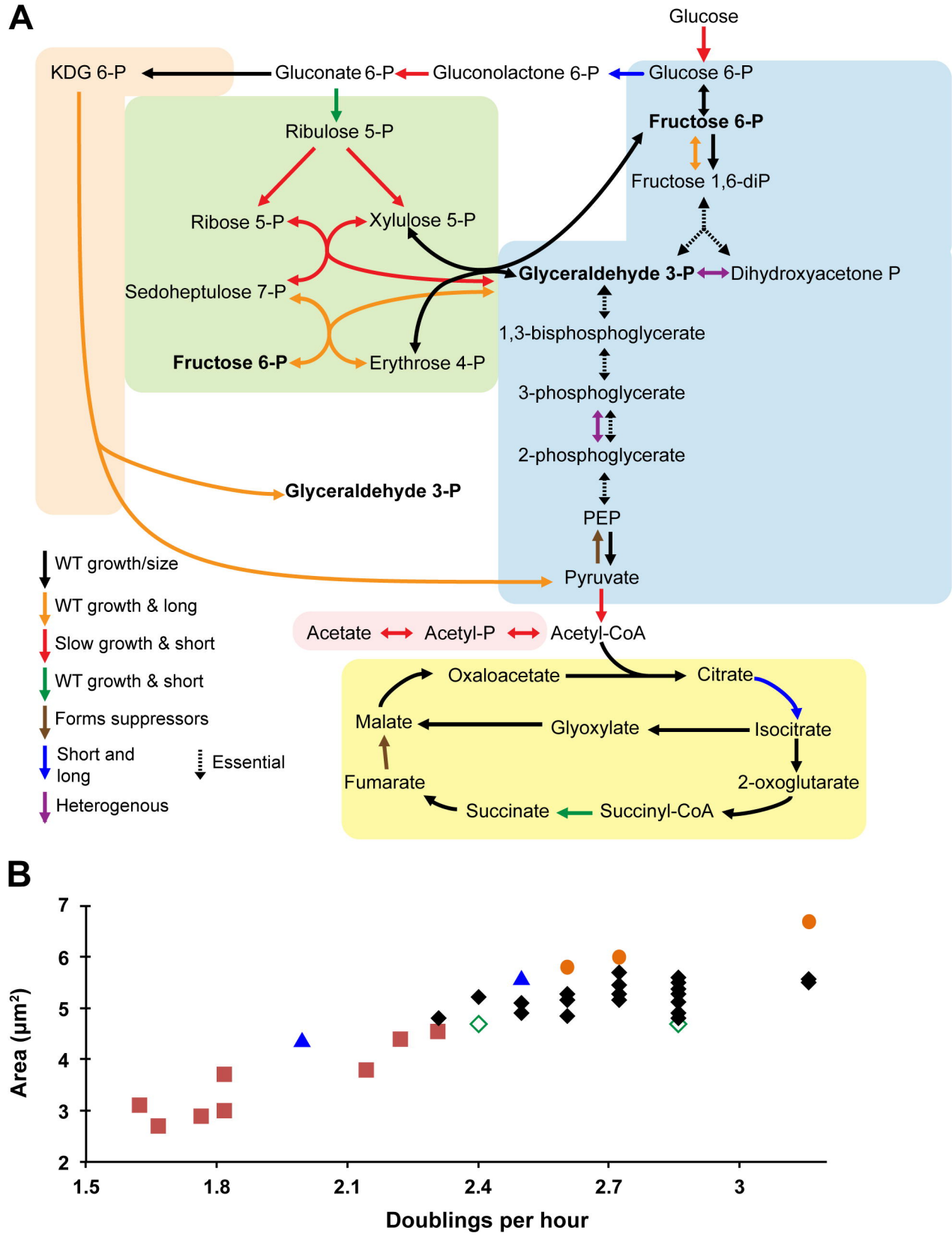
A
Glucose
KDG 6-P
Gluconate 6-P
Gluconolactone 6-P
Glucose 6-P
Fructose 6-P
Fructose 1,6-diP
Ribulose 5-P
Ribose 5-P
Xylulose 5-P
Sedoheptulose 7-P
Fructose 6-P
Erythrose 4-P
Glyceraldehyde 3-P
Dihydroxyacetone P
1,3-bisphosphoglycerate
3-phosphoglycerate
2-phosphoglycerate
PEP
Pyruvate
Glyceraldehyde 3-P
Acetate
Acetyl-P
Acetyl-CoA
Oxaloacetate
Citrate
Isocitrate
2-oxoglutarate
Succinyl-CoA
Succinate
Fumarate
Malate
Glyoxylate
WT growth/size
WT growth & long
Slow growth & short
WT growth & short
Forms suppressors
Short and long
Essential
Heterogenous
B
Area (μm²)
Doublings per hour
7
6
5
4
3
2
1.5
1.8
2.1
2.4
2.7
3

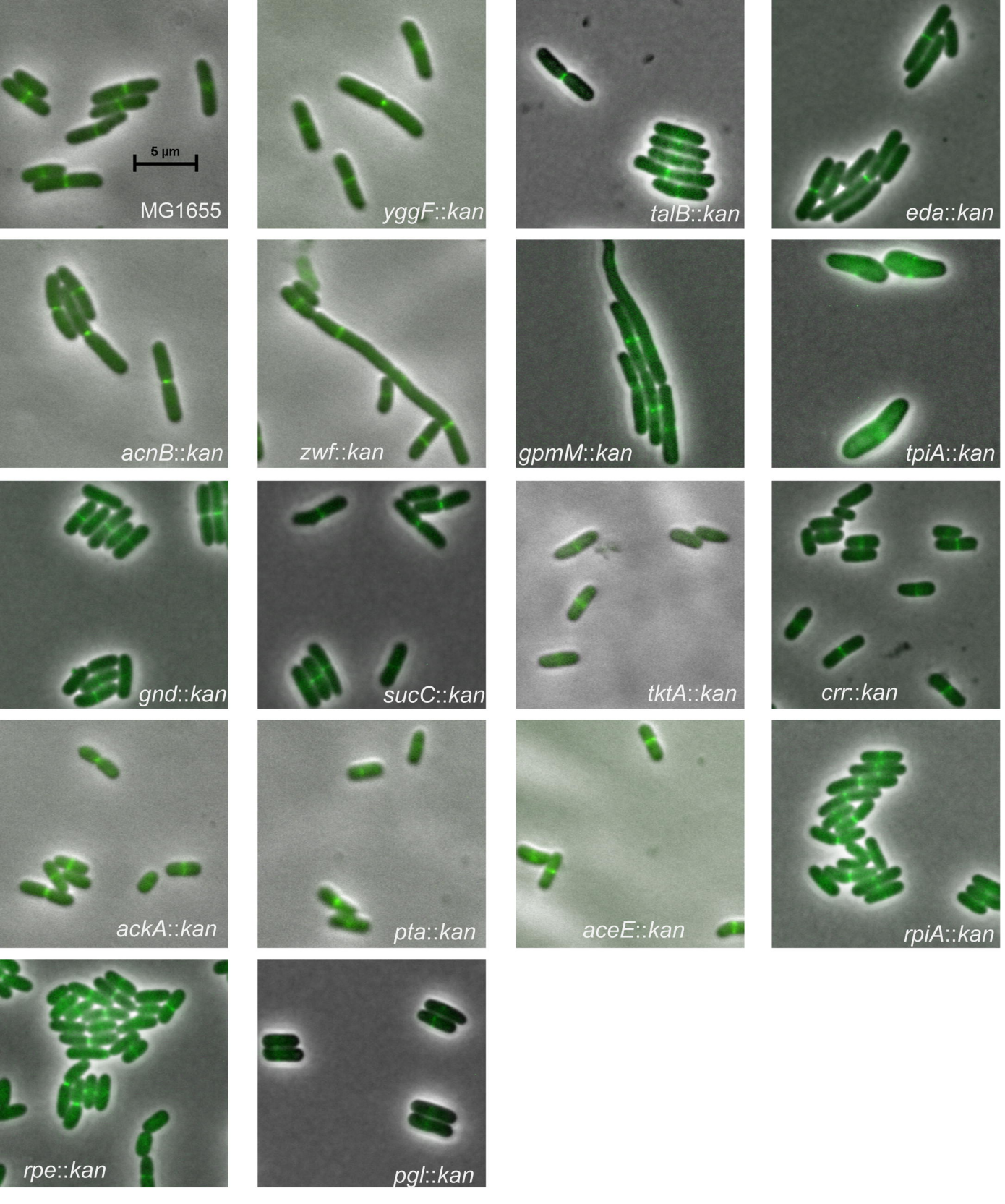
5 µm
MG1655
yggF::kan
talB::kan
eda::kan
acnB::kan
zwf::kan
gpmM::kan
tpiA::kan
gnd::kan
sucC::kan
tktA::kan
crr::kan
ackA::kan
pta::kan
aceE::kan
rpiA::kan
rpe::kan
pgl::kan

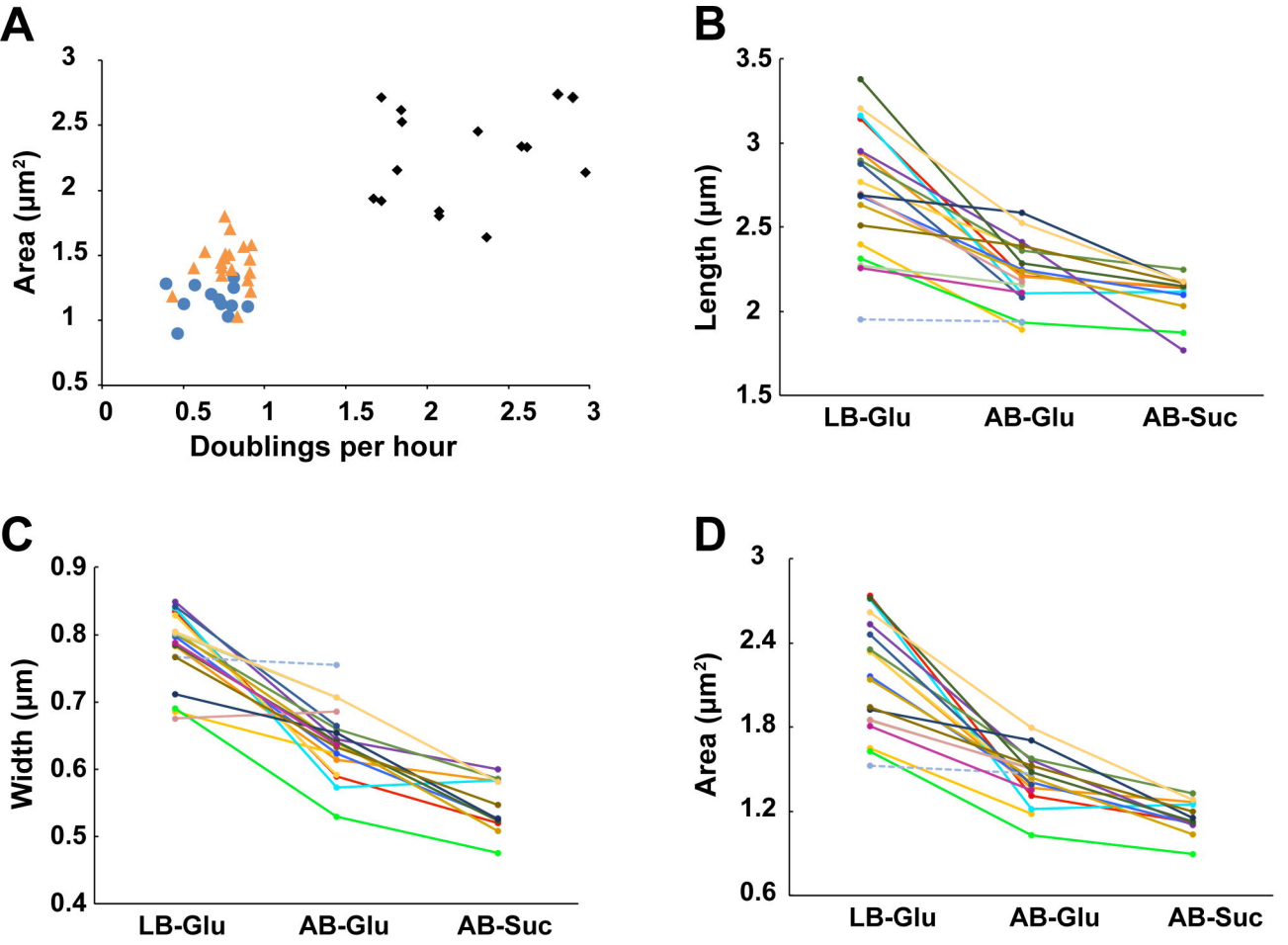
A
Area (μm²)
Doublings per hour
B
Length (μm)
LB-Glu
AB-Glu
AB-Suc
C
Width (μm)
LB-Glu
AB-Glu
AB-Suc
D
Area (μm²)
LB-Glu
AB-Glu
AB-Suc

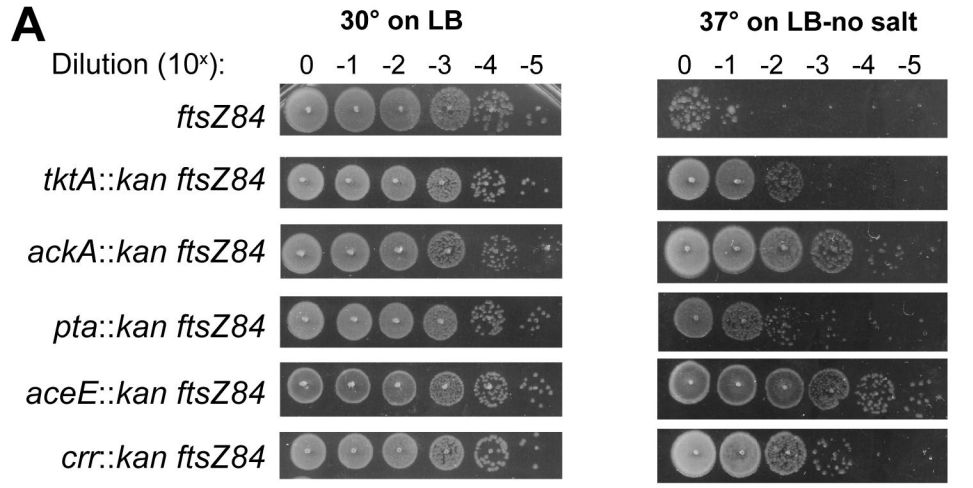
A
30° on LB
37° on LB-no salt
Dilution (10x):
0 -1 -2 -3 -4 -5
ftsZ84
tktA::kan ftsZ84
ackA::kan ftsZ84
pta::kan ftsZ84
aceE::kan ftsZ84
crr::kan ftsZ84

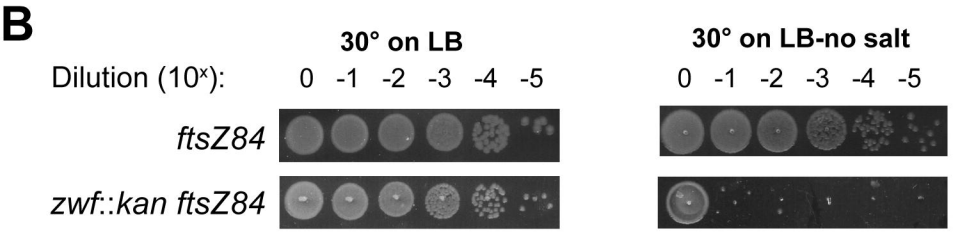
B
30° on LB
30° on LB-no salt
Dilution (10x):
0 -1 -2 -3 -4 -5
ftsZ84
zwf::kan ftsZ84

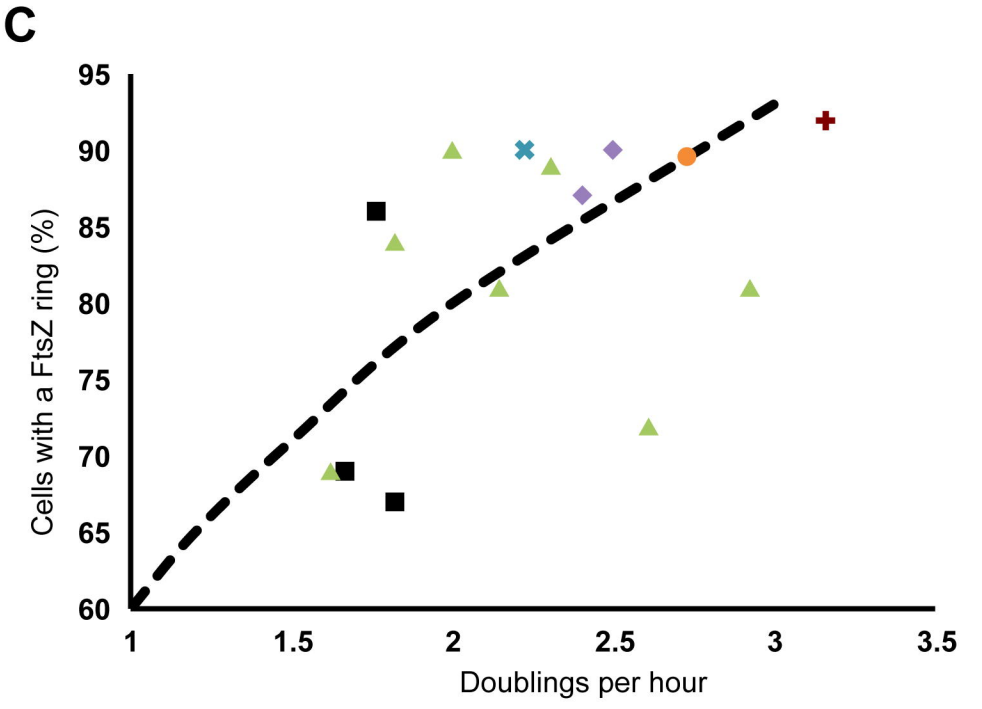
C
Cells with a FtsZ ring (%)
95
90
85
80
75
70
65
60
1
1.5
2
2.5
3
3.5
Doublings per hour

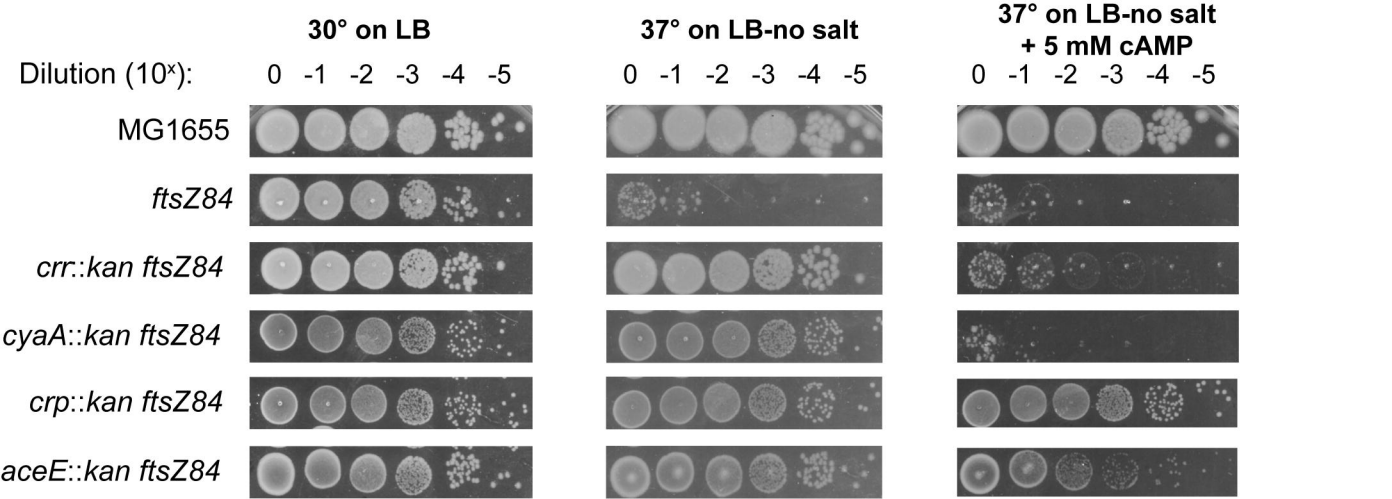
30° on LB
37° on LB-no salt
37° on LB-no salt
+ 5 mM cAMP
Dilution (10x):
0 -1 -2 -3 -4 -5
0 -1 -2 -3 -4 -5
0 -1 -2 -3 -4 -5
MG1655
ftsZ84
crr::kan ftsZ84
cyaA::kan ftsZ84
crp::kan ftsZ84
aceE::kan ftsZ84

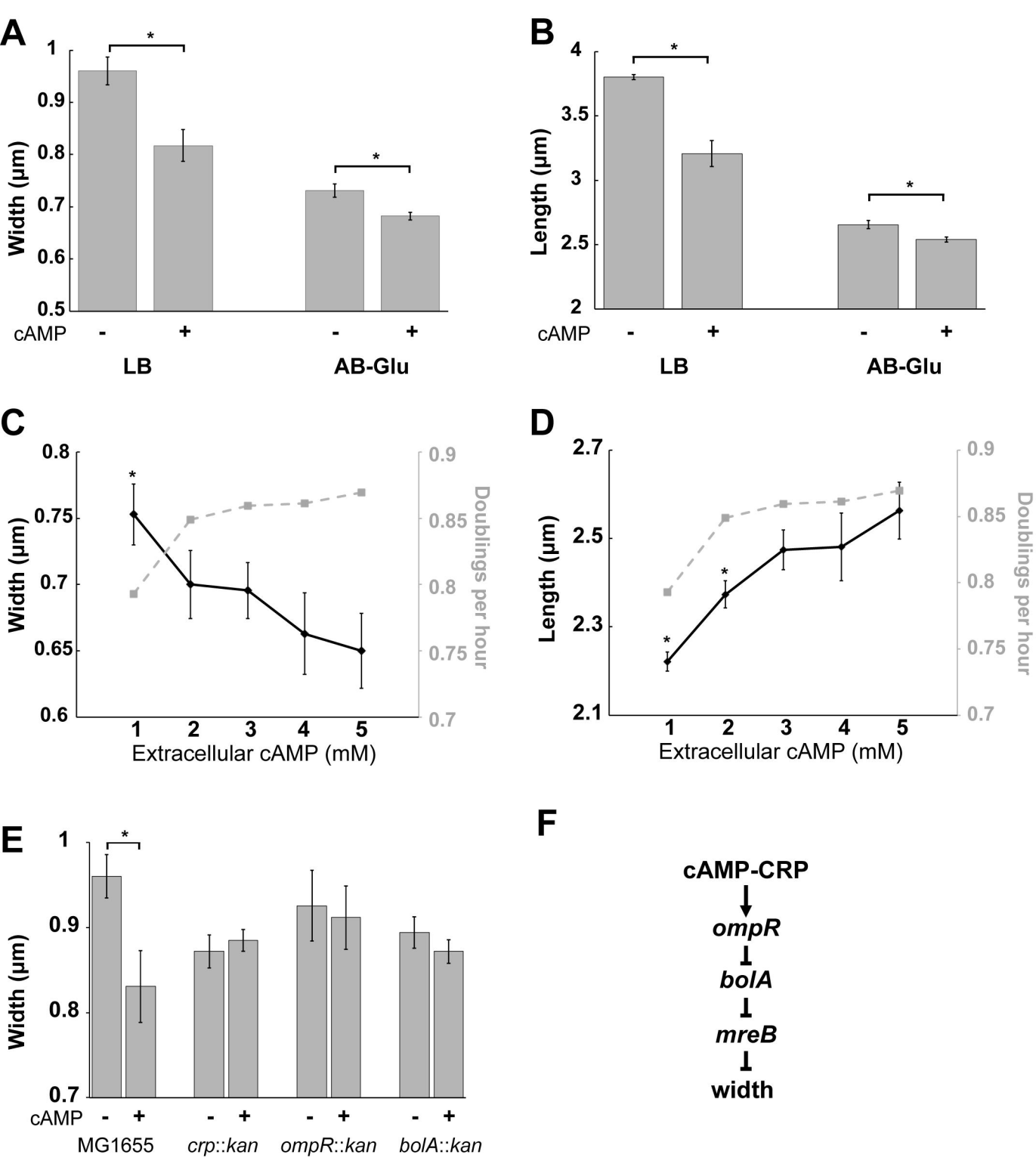
A
Width (µm)
1
0.9
0.8
0.7
0.6
0.5
*
*
cAMP
-
+
-
+
LB
AB-Glu
B
Length (µm)
4
3.5
3
2.5
2
*
*
cAMP
-
+
-
+
LB
AB-Glu
C
Width (µm)
0.8
0.75
0.7
0.65
0.6
Doublings per hour
0.9
0.85
0.8
0.75
0.7
*
1
2
3
4
5
Extracellular cAMP (mM)
D
Length (µm)
2.7
2.5
2.3
2.1
Doublings per hour
0.9
0.85
0.8
0.75
0.7
*
*
1
2
3
4
5
Extracellular cAMP (mM)
E
Width (µm)
1
0.9
0.8
0.7
*
cAMP
-
+
-
+
-
+
-
+
MG1655
crp::kan
ompR::kan
bolA::kan
F
cAMP-CRP
ompR
bolA
mreB
width

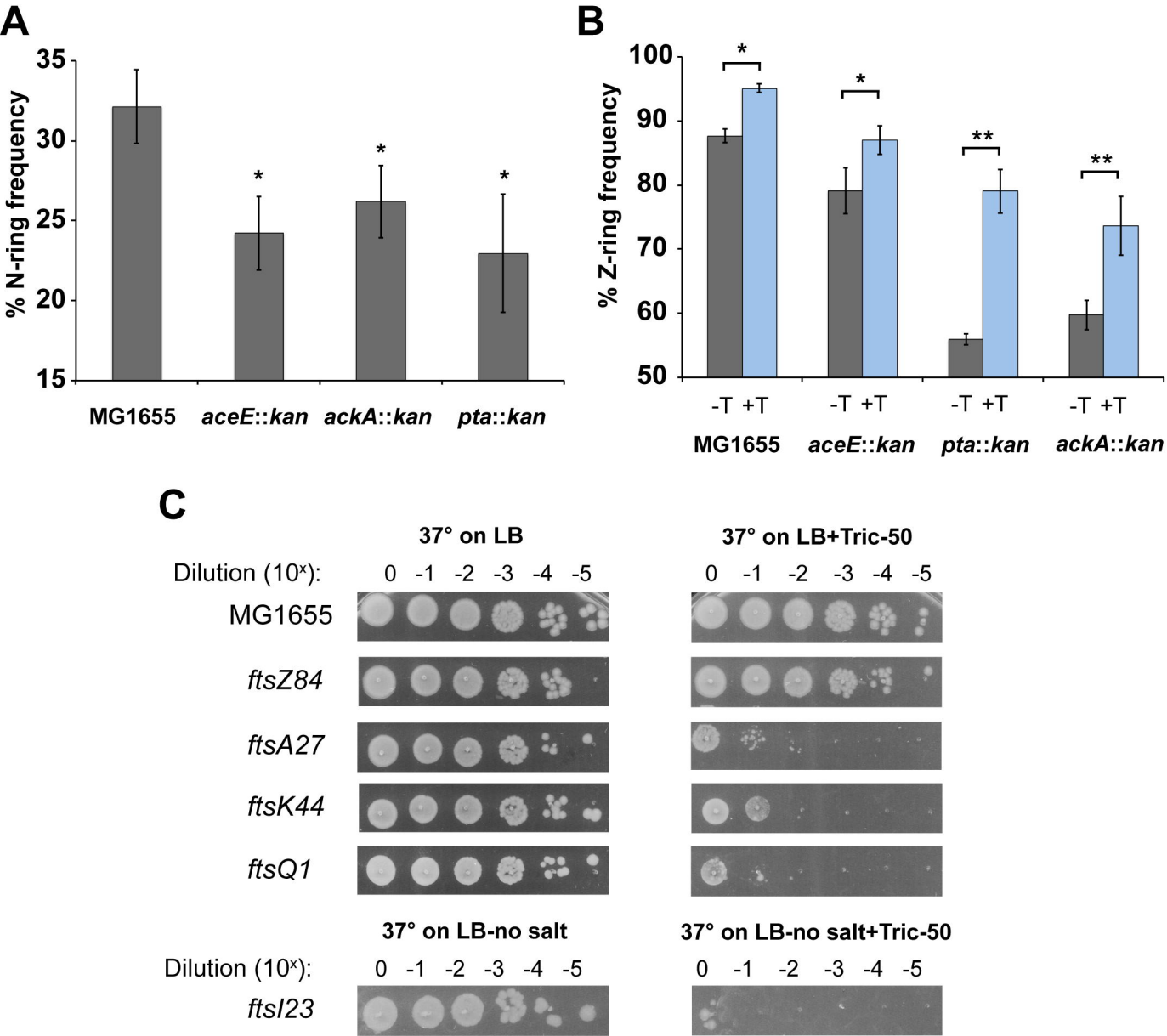
A
% N-ring frequency
35
30
25
20
15
*
*
*
MG1655
aceE::kan
ackA::kan
pta::kan
B
% Z-ring frequency
100
90
80
70
60
50
*
*
**
**
-T +T
-T +T
-T +T
-T +T
MG1655
aceE::kan
pta::kan
ackA::kan
C
37° on LB
37° on LB+Tric-50
Dilution (10x):
0 -1 -2 -3 -4 -5
MG1655
ftsZ84
ftsA27
ftsK44
ftsQ1
37° on LB-no salt
37° on LB-no salt+Tric-50
Dilution (10x):
0 -1 -2 -3 -4 -5
ftsI23

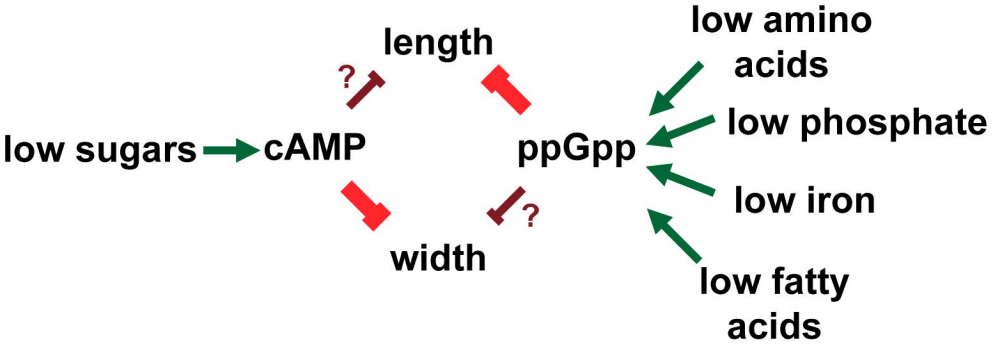
length
?
low amino acids
low sugars
cAMP
ppGpp
low phosphate
low iron
?
width
low fatty acids